Eur Biophys J (2010) 39:277–287
DOI 10.1007/s00249-009-0537-7

ORIGINAL PAPER

Minimal models of electric potential oscillations in non-excitable membranes

Guillermo Perdomo · Julio A. Hernández

Received: 30 April 2009 / Revised: 21 August 2009 / Accepted: 26 August 2009 / Published online: 18 September 2009

Abstract Sustained oscillations in the membrane potential have been observed in a variety of cellular and subcellular systems, including several types of non-excitable cells and mitochondria. For the plasma membrane, these electrical oscillations have frequently been related to oscillations in intracellular calcium. For the inner mitochondrial membrane, in several cases the electrical oscillations have been attributed to modifications in calcium dynamics. As an alternative, some authors have suggested that the sustained oscillations in the mitochondrial membrane potential induced by some metabolic intermediates depends on the direct effect of internal protons on proton conductance. Most theoretical models developed to interpret oscillations in the membrane potential integrate several transport and biochemical processes. Here we evaluate whether three simple dynamic models may constitute plausible representations of electric oscillations in non-excitable membranes. The basic mechanism considered in the derivation of the models is based upon evidence obtained by Hattori et al. for mitochondria and assumes that an ionic species (i.e., the proton) is transported via passive and active transport systems between an external and an internal compartment and that the ion affects the kinetic properties of transport by feedback regulation. The membrane potential is incorporated via its effects on kinetic properties. The dynamic properties of two of the models enable us to conclude that they may represent alternatives enabling description of the generation of electrical oscillations in membranes that depend on the transport of a single ionic species.

Keywords Membrane potential · Mathematical models · Oscillations · Ionic transport

G. Perdomo · J. A. Hernández (✉)
Sección Biofísica, Facultad de Ciencias,
Universidad de la República,
Iguá esq. Mataojo, 11400 Montevideo, Uruguay
e-mail: jahern@fcien.edu.uy

Introduction

Periodic modifications in plasma membrane potential constitute the physical basis for the properties of neural and muscular tissues. Oscillations in the electric potential difference across membranes can also be observed in a variety of other cellular systems, for example pancreatic beta cells (Magnus and Keizer 1998; Bergsten 2002; Manning Fox et al. 2006; Nunemaker et al. 2006), HeLa cells (Tilly et al. 1990), macrophages (Hanley et al. 2004), lens epithelial cells (Thomas et al. 1998), cultured fibroblasts expressing the Ha-ras oncogene (Lang et al. 1991), mitochondria (Vergun et al. 2003; Cortassa et al. 2004; Vergun and Reynolds 2004; Hattori et al. 2005), and unicellular organisms (Bauer et al. 1999). In many cases these electrical responses take the form of sustained oscillations associated with oscillations in intracellular calcium, as occurs, for instance, in the beta cells of the islets of Langerhans in response to increases in extracellular glucose (Manning Fox et al. 2006; Nunemaker et al. 2006). Depending on the particular cell type, diverse other factors may promote oscillations in the cell membrane potential (e.g., ATP (Hanley et al. 2004), bradykinin (Lang et al. 1991), histamine (Tilly et al. 1990), acetylcholine (Thomas et al. 1998), and xanthines (Bauer et al. 1999)). In isolated mitochondria oscillations in the electric potential difference across the inner membrane (V_m) may be triggered by Ca^{2+} (Krippeit-Drews et al. 2000; Vergun and Reynolds 2004; Chalmers and McCarron 2008) and by malate or

succinate (Hattori et al. 2005). A proposed mechanism for the oscillations in V_m in mitochondria assumes a direct effect of mitochondrial pH on the proton conductance of the inner membrane (Hattori et al. 2005). Theoretical studies of membrane potential oscillations have been developed for pancreatic beta cells (Magnus and Keizer 1998) and for mitochondria (Cortassa et al. 2004) by use of explicit models integrating several transport and biochemical mechanisms.

The purpose of this study was to evaluate whether some simple dynamic models may constitute plausible representations of membrane potential oscillations in non-excitable membranes. In essence, the models are based on the findings and interpretations described by Hattori et al. (2005) for mitochondria and assume that the passive and active transport of a single ionic species (e.g., the proton) across a membrane is essentially responsible for the electrical oscillations. As the basis for oscillatory behavior the models do not assume the presence of voltage-gated channels, characteristic of excitable cells, but the direct effect of the transported ion on the transport kinetics. The first model considered (Model I) is directly based on the interpretation of Hattori et al. (2005) of their experimental findings and assumes the existence in the inner mitochondrial membrane of a proton channel that transits from a closed to an open state in response to matrix alkalinization. The second model (Model II) is a continuous version of the discrete Model I and assumes that the increase in intramitochondrial proton concentration is capable of inactivating the proton channel. Model III is also a continuous model that, from a formal point of view, is similar to the classical Higgins model developed to interpret oscillations in biochemical systems (Higgins 1964, 1967). The membrane potential is incorporated via its effects on some kinetic properties. From the analysis and numerical simulations we conclude that Models I and III are capable to represent oscillatory behavior, whereas Model II is not. In Models I and III, the induction of oscillations is achieved under conditions that mimic the participation of effectors (i.e., energetic metabolites), as reported by Hattori et al. (2005). We conclude that these models are consistent with available evidence and may well constitute minimal models capable of representing sustained oscillations in the membrane potential of non-excitable cells associated with the transport of a single ionic species.

Dynamic models

General characteristics of the mechanisms of cation transport

As mentioned above, the models introduced here are based upon the findings of Hattori et al. (2005, henceforth referred to as HWU) about the occurrence of membrane potential oscillations in single isolated mitochondria. According to these authors, the essential oscillatory behavior solely requires the interaction of two processes of proton transport across the inner mitochondrial membrane:

1 proton pumping by intermediates of the respiratory chain, and
2 passive entry of protons by a conductance path sensitive to pH modifications.

The transport model employed here to derive the mathematical models follows these basic ideas (Fig. 1). In essence, we consider a non-excitable membrane containing the systems responsible for the active and passive transport of a single cationic species (e.g., the proton). Although every step of the overall process is reversible, we assume here that the membrane potential-independent section of the model operates in an irreversible fashion. For Model I, we consider the ion to be transported from the external compartment (at concentration x_o) to the internal compartment (at concentration y) in a one-step process. For Models II and III, this passive transport of the cation occurs in a two-step process (Fig. 1a), where it is first transported by system 2 from the external compartment (at concentration x_o) towards an intermediate intra-membrane state (at concentration x) and then from this intermediate state towards the internal compartment (at concentration y) by system 3. System 1 pumps the cation from the internal towards the external compartment and is the cause of the irreversible operation of this section. We assume that the

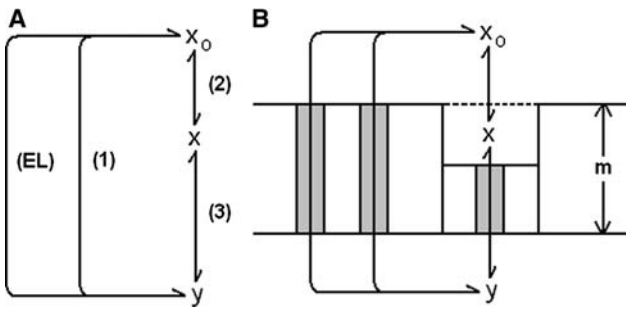

Fig. 1 Diagram of the ion transport processes across the membrane. **a** The ion is transported from the external compartment (at constant concentration x_o) to the internal compartment (at variable concentration y). Through the paths on the left of the scheme (*1* and *EL*), the ion is directly transported between the two compartments. Through the path on the right, the ion can be transported by a one (Model I) or two-step (Models II and III) process, x being an intermediate state between transport steps *2* and *3*. Paths *1*, *2* and *3* are electroneutral; *EL* denotes an electrogenic path. **b** A possible mechanistic model of the events represented by the scheme in **a**. Paths *1* and *EL* could correspond to active transport systems driving the ion from the internal to the external compartment. The intermediate state x could be the consequence of the existence of a membrane compartment acting as a vestibule for the ion, as has been suggested for several ionic channels (see main text)

other pumping system, EL, functions reversibly. The external concentration of the cation (x_o) is a parameter. The total membrane densities of the transport proteins are implicitly considered to remain constant. The concentration of the intermediate state (x), the internal concentration (y), and the electric potential difference across the membrane (V_m) represent the dependent variables. In this respect, we assume that V_m is only determined by the transport of the cation by the electrogenic system (EL). Attempts to obtain oscillatory behavior of Model III by incorporating the voltage dependence solely on the basis of the kinetic properties of systems 1 and 3 were unsuccessful (not shown). Figure 1b shows a possible mechanistic counterpart to the kinetic scheme of Fig. 1a. For the case of proton transport across the inner mitochondrial membrane, both systems 1 and EL would correspond to proton-pumping sites of the respiratory chain (Nicholls and Budd 2000). The intermediate state x could be determined by the existence of a wide vestibule at the external site of the channel (Aidley and Stanfield 1996). "System 2" would thus correspond to cation diffusion from the external compartment towards the channel vestibule. As mentioned, the existence of the corresponding putative proton channel has been proposed by HWU in agreement with their experimental evidence. It should be noted that the schematic model shown in Fig. 1 is not intended to constitute a minimal representation of the diverse aspects of energy coupling in membranes, a rather complex matter analyzed elsewhere (see, for instance, Nicholls and Ferguson 2002), but to suggest a basic mechanism for the generation of electrical oscillations in this type of membrane.

All the models studied here consider the existence of a feedback effect of the transported ion on the ion conductance. This assumption is based upon the finding by HWU of pH regulation of the proton influx towards the mitochondrial matrix. Feedback modulation by the transported ion has been encountered in several proton channels (Decoursey 2003) and also in a wide variety of calcium channels (Lee and Catterall 2005), a fact that makes it possible that models similar to those developed here could also be considered to account for calcium oscillations.

Incorporation of the membrane potential

As mentioned above, we have assumed that the processes mediated by transport systems 1, 2, and 3 (Fig. 1a) are independent of the membrane potential and that an accessory electrogenic process (EL) operates reversibly, transporting the ion between the two compartments. The ion flux mediated by this system is:

$$J_{ion} = \mu x_o - \eta y. \quad (1)$$

The kinetic parameters μ and η are affected by the electrical potential difference across the membrane (V_m, defined as $V_{outside} - V_{inside}$) according to the relationships:

$$\mu = \mu_0 \exp(FV_m/2RT)$$

$$\eta = \eta_0 \exp(-FV_m/2RT)$$

where μ_0 and η_0 are V_m-independent and where F is Faraday's constant, R the gas constant, and T the absolute temperature (310 K).

Assuming that EL operates in an overall electroneutral fashion, we calculated the membrane potential difference after each time step of the numerical integration process employing the equation (Hernández et al. 1989; Hernández 2003):

$$V_m = (RT/F) \ln(\eta_0 y/\mu_0 x_o) \quad (2)$$

In general, the rate of change of y (dy/dt) would be given by:

$$dy/dt = F + \psi(\mu x_o - \eta y),$$

where the function F depends on the particular model considered and where ψ is a parameter. For the cases analyzed here, the electroneutral condition implies that the term $\mu x_o - \eta y$ is nil (cf. Eqs. 1 and 2) and therefore does not affect the dynamics of y.

Finally, we considered that η_0 is a function of the concentration of an energetic metabolite M (e.g., malate or succinate) according to the equation:

$$\eta_0 = n_0 + n_1 M \quad (3)$$

where n_0 and n_1 are parameters.

Model I

As mentioned above, this model is directly based on the mechanism of generation of electrical oscillations in mitochondria suggested by HWU. On the basis of their experimental evidence, these authors proposed that proton entry is mediated by a channel that opens in response to matrix alkalinization caused by enhanced proton pumping, in turn determined by incorporation of M in the incubation medium. The simplest dynamic model describing this mechanism is:

$$dy/dt = \alpha - \delta y, \quad (4)$$

where α and δ are parameters representing the rates of proton entry and proton pumping, respectively. As already mentioned, this model must account for the effect observed by HWU in response to incorporation of additional metabolites (e.g., malate or succinate) in the experimental medium. For this purpose, we assumed that α and δ have the following dependences on the threshold concentration of y (y_{th}) and on the concentration of the added metabolite (M):

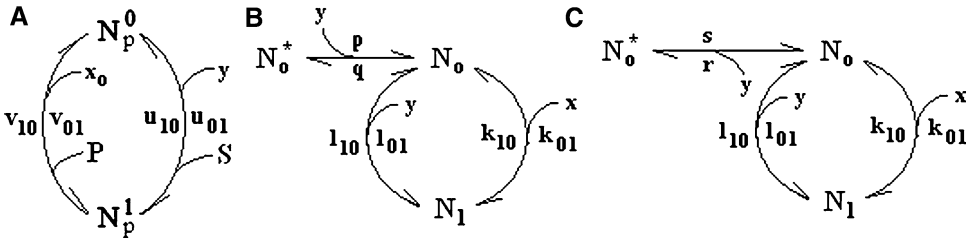

Fig. 2 Kinetic diagrams describing a pump coupling the transport of the cation to the reaction S ↔ P (**a**), a channel activated by y (**b**), and a channel inactivated by y (**c**). N_p^0 and N_p^1 are intermediate states of the enzyme (**a**); N_o*, N_o and N_1 are intermediate states of the channels (**b** and **c**); u_{01}, v_{10}, u_{10}, and v_{01} (**a**), and p, q, r, s, k_{01}, l_{10}, k_{10}, and l_{01} (**b** and **c**) are true rate constants

$$\alpha = (\alpha_0 + \alpha_1)x_o$$
$$\delta = \delta_0 + \delta_1 M \tag{5}$$

If $y < y_{th}$, $\alpha_1 = \alpha_1^0$; if $y \geq y_{th}$, $\alpha_1 = 0$.

In Eqs. (5), α_0, α_1^0, δ_0, and δ_1 are parameters. For α, Eqs. (5) imply there are two components of proton conductance, one insensitive to pH changes (α_0) and the other triggered by matrix alkalinization (α_1). Similarly, the cation pumping rate (δ) has two components, only one of which (δ_1) is related to the effect of the metabolite M. Depending upon the values of the parameters, Model I may behave as follows. From Eqs. 4 and 5, if $M \neq 0$ and y is larger than the threshold value (y_{th}), y will decrease until it reaches y_{th}. At this point, the additional proton conductance provided by the term α_1^0 is triggered and y increases until it balances the pumping term. When this occurs, a new cycle begins. The model may thus behave in accordance with HWU's interpretations of their experimental findings. It should be noted that in Model I the term for active transport of the cation does not include saturation effects.

Model II

This model represents an attempt to obtain a continuous and more general version of the discrete Model I. For this purpose we have assumed that y affects the transport system 3 (Fig. 1a) by negative feedback regulation and that the transport system 1 exhibits saturation kinetics. In Appendix 1 we derive the expression for active transport of the cation from analysis of a simple kinetic model of a cation pump (Fig. 2a). A decrease in y (i.e., matrix alkalinization) would cause an increase in proton channel activity, as assumed for Model I in an all-or-none fashion. Under these assumptions, the mathematical model governing the velocity of change of x and y is:

$$dx/dt = \alpha - [\beta x/(1 + \varphi y)]$$
$$dy/dt = [\beta x/(1 + \varphi y)] - [\delta y/(1 + \gamma y)]. \tag{6}$$

where α, β, γ, δ, and φ are parameters and where we have employed a simple kinetic expression to account for the negative feedback effect of y on the flux mediated by system 3. In Appendix 2 we derive this expression from analysis of an explicit kinetic model of channel inactivation (Fig. 2c).

A non-dimensional version of the model given by Eq. 6 can be obtained by introducing the definitions:

$$m = \gamma x$$
$$n = \gamma y$$
$$k = (\beta\delta/\alpha\gamma)/(\delta - \alpha\gamma + \alpha\varphi) \tag{7}$$
$$r = \delta/(\alpha\gamma)$$
$$\tau = \alpha\gamma t$$

From these definitions, Model II (Eq. 6) can be transformed into the following non-dimensional model:

$$dm/d\tau = 1 - km/(1 + n)$$
$$dn/d\tau = km/(1 + n) - rn/(1 + n). \tag{8}$$

The steady state (m*, n*) is given by:

$$m^* = (r/k)/(r - 1)$$
$$n^* = 1/(r - 1) \tag{9}$$

From Eq. 9, the physically meaningful solutions require that $k > 0$ and $r > 1$. Stability analysis of the non-dimensional version of Model II is performed in Appendix 3. From this analysis, we conclude that Model II is not capable of exhibiting oscillatory behavior (cf. Eq. 27).

Model III

For this model we assumed that y affects transport system 3 (Fig. 1a) by positive feedback regulation and that, similarly to Model II, transport system 1 exhibits saturation kinetics. Under these assumptions, the mathematical model governing the velocity of change of x and y is:

$$dx/dt = \alpha - \beta xy.$$
$$dy/dt = \beta xy - [\delta y/(1 + \gamma y)] \tag{10}$$

where α, β, γ and δ are parameters and where we have employed a simple kinetic expression to account for the

positive feedback effect of y on the flux mediated by system 3. In Appendix 2 we derive this expression from analysis of an explicit kinetic model of channel activation (Fig. 2b). It should be noted that the dynamic model given by Eq. 10 is formally similar to the classical minimal Higgins Model, developed to describe glycolytic oscillations (Higgins 1964, 1967; McDonald 2003).

We considered that α, β, γ, and δ have the following dependences on the external concentration of the cation (x_o) and on the concentration of the energetic metabolite (M), respectively:

$$\begin{aligned}\alpha &= \kappa x_o,\\ \beta &= b_0/x_o^2 + b_1 M/x_o^2\\ \gamma &= c_0/x_o + c_1 M/x_o\\ \delta &= d_0/x_o + d_1 M/x_o,\end{aligned} \tag{11}$$

where κ, b_0, b_1, c_0, c_1, d_0 and d_1 are parameters. The effect of M on δ is analogous to that considered for Model I (cf. Eq. 5) and consistent with the expression for the active flux obtained from analysis of a simple model of a cation pump (cf. Eq. 21). The effect of x_o on δ and γ is consistent with Eq. 21. It should be noted that, following the interpretation of HWU, this effect has not been considered for the case of Model I. For the numerical simulations we assumed that c_1 is negligible and, consequently, that M does not significantly affect γ, an assumption that provided a better numerical approximation to the experimental evidence. The effect of M on β is arbitrary and has also been introduced to obtain a better approximation to the experimental results. The dependence of β on x_o enables introduction of the effect of alkalinization on cation conductance, similarly to that considered in Model I to account for the experimental evidence (cf. Eqs. (5)).

The steady state (x^*, y^*) of Model III is given by:

$$\begin{aligned}x^* &= (\delta - \alpha\gamma)/\beta\\ y^* &= \alpha/(\delta - \alpha\gamma).\end{aligned} \tag{12}$$

A non-dimensional version of Model III can be obtained by introducing the following definitions:

$$\begin{aligned}m &= \gamma x\\ n &= \gamma y\\ k &= \beta/(\alpha\gamma^2)\\ r &= \delta/(\alpha\gamma)\\ \tau &= \alpha\gamma t\end{aligned} \tag{13}$$

From these definitions, the model given by Eq. 10 can be transformed into the following non-dimensional model:

$$\begin{aligned}dm/d\tau &= 1 - kmn\\ dn/d\tau &= kmn - rn/(1+n).\end{aligned} \tag{14}$$

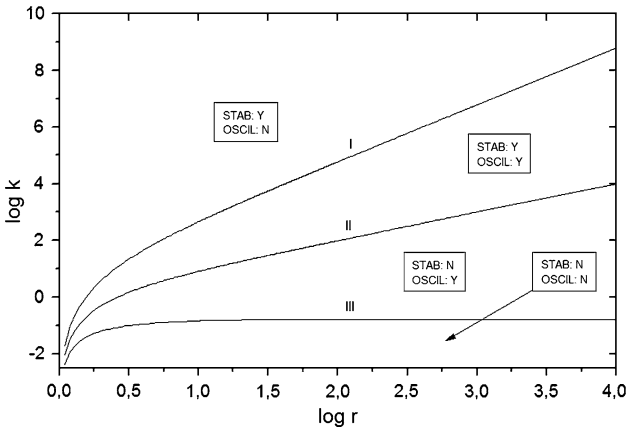

Fig. 3 Stability diagram of Model III. The *plot* shows the stability regions as functions of the non-dimensional terms k and r (Eqs. 13–15).*Curves I* and *III* correspond to the solutions of $\Delta = 0$ whereas *curve I* corresponds to the solution of $\theta = 0$ (Eq. 28). According to the dynamic behavior, the plane (k, r) has been divided into four regions, each one displaying the existence (Y) or non-existence (N) of stability (*STAB*) and oscillations (*OSCIL*)

The steady state (m^*, n^*) of the non-dimensional version of Model III is given by

$$\begin{aligned}m^* &= (r-1)/k.\\ n^* &= 1/(r-1)\end{aligned} \tag{15}$$

From the above, the steady-state expressions for the original variables (Eq. 12) can be alternatively obtained by employing Eqs. 13 and 15. Inspection of Eq. 15 reveals that a physically meaningful solution requires $k > 0$ and $r > 1$.

Stability analysis of the non-dimensional version of Model III is performed in Appendix 3. From these studies we conclude that Model III is capable of exhibiting oscillatory behavior over a significant range of values of k and r, as emerges from inspection of the stability regions on the plane (k, r; Fig. 3). From this analysis we also conclude that, for $r \gg 1$, the bifurcation point corresponds to $r = k$ (Eq. 28). For this condition, the period of sustained oscillations is given by Eq. 29.

Numerical results and discussion

For illustrative purposes, we performed numerical simulations of Models I and III for a hypothetical microorganism or for mitochondria performing active (i.e., mediated by system 1 and the accessory electrogenic system EL, Fig. 1a) and passive (i.e., mediated by systems 2 and 3) transport of protons across the membrane. Model II is not taken into consideration because, as concluded above, it is not capable of exhibiting oscillatory behavior. Because, as also remarked above, the models are not intended to

Table 1 Numerical values of the parameters

Model I	
$\alpha_0 = 10^{-5}\ s^{-1}$	$\alpha_1^0 = 0.7\ s^{-1}$
$\delta_0 = 10^{-4}\ s^{-1}$	$\delta_1 = 2.4 \times 10^3\ mol^{-1}\ cm^3\ s^{-1}$
$y_{th} = 6.44 \times 10^{-12}$ mol cm^{-3} ($pH_{th} = 8.2$)	
Model III	
$\kappa = 0.1\ s^{-1}$	
$b_0 = 10^{-12}$ mol cm^{-3}	$b_1 = 2 \times 10^{-6}\ s^{-1}$
$c_0 = 0.1$	
$d_0 = 10^{-11}$ mol cm^{-3} s^{-1}	$d_1 = 2 \times 10^{-5}\ s^{-1}$
Other variables	
$\mu_0 = 1$ cm s^{-1}	
$n_0 = 10^2$ cm s^{-1}	$n_1 = 10^9\ mol^{-1}\ cm^4\ s^{-1}$
$x_o = 10^{-10}$ mol cm^{-3} ($pH_o = 7.0$)	
$M = 5 \times 10^{-6}$ mol cm^{-3} (= 5 mM)	

represent sufficiently complete descriptions of the overall properties of the mechanisms of energy coupling in mitochondria or microorganisms, the participation of other specific processes (e.g., action of F_oF_1 ATPases, production of reactive oxygen species, dynamics of mitochondrial calcium storage, etc.) has not been considered. The literature offers several examples of detailed models of the energetics of mitochondria and microorganisms (see, for instance, Cristina and Hernández 2000; Cortassa et al. 2003; Beard 2005; Bertram et al. 2006). In this respect, the main objective of the numerical simulations performed here was to reproduce some of the experimental findings specifically reported by HWU. To the best of our knowledge, there are no further studies on mitochondrial oscillations reporting results obtained under similar experimental conditions to those employed by these authors. In particular, the simulations performed here intended to reproduce the finding by HWU that some metabolites (e.g., malate or succinate) can trigger electrical oscillations in isolated mitochondria. Other theoretical studies describing mitochondrial oscillations incorporate the effects of other mitochondrial processes, for example the dynamics of calcium storage (Vergun and Reynolds 2004) or the production of reactive oxygen species (Cortassa et al. 2004). As mentioned above, under their experimental conditions, HWU interpreted their evidence attributing the oscillatory behavior solely to the interaction between the active and passive transport of protons.

Choice of numerical values of the variables

To determine the reference state for each model we utilized the numerical values of the parameters listed in Table 1. This choice of parameters was based on two restrictive criteria—a mitochondrial pH between 7 and 9 (corresponding to y^* between 10^{-10} and 10^{-12} mol cm^{-3}) and a potential difference V_m across the membrane between 0.10 and 0.20 V. These values fall within the range of those typically found in mitochondria and diverse microorganisms (Tedeschi 1974; Miller and Koshland 1977; Brand and Felber 1984; Chen 1988; Nicholls and Budd 2000). In addition, another aspect considered here is that the parameters chosen should yield oscillatory behavior similar to that experimentally encountered by diverse authors (Cortassa et al. 2004; Vergun and Reynolds 2004; Hattori et al. 2005). From the available evidence, we imposed a period of ~ 60 s for the sustained oscillations triggered by the metabolite M at a concentration of 5 mM. This value corresponds to a frequency that falls within the range of those reported by those authors. Finally, we considered that the reference external concentration of the cation would be $x_o = 10^{-10}$ mol cm^{-3}, corresponding to an external pH = 7.

For the particular case of Model III, we also imposed a time unit s for the original model equal to 1 s (yielding a time unit h for the non-dimensional model equal to $\alpha\gamma$, cf. Eq. 13). This and the above restrictions imply the following for Model III (cf. Eqs. 13 and 15):

$$\begin{aligned} &\alpha/(\delta - \alpha\gamma) = 10^{-11}\,\mathrm{mol\,cm^{-3}} \\ &\alpha\gamma s = h. \\ &s = 1\,\mathrm{s} \end{aligned} \tag{16}$$

From Eqs. 13, 15 and 16, we obtain the following expressions for the original parameters of Model III:

$$\begin{aligned} \alpha &= 10^{-11} h\,(r-1)\,\mathrm{mol\,cm^{-3}\,s^{-1}} \\ \beta &= 10^{11} hk/(r-1)\,\mathrm{mol^{-1}\,cm^3\,s^{-1}} \\ \gamma &= 10^{11}/(r-1)\,\mathrm{mol^{-1}\,cm^3} \\ \delta &= hr\,\mathrm{s^{-1}} \end{aligned} \tag{17}$$

From the above assumptions we obtained, from Eqs. 16 and 17, the numerical values for the parameters of Model III shown in Table 1. Figure 4 shows the dependence of the steady state values of pH_i and V_m on the concentration of the metabolite (M) for the particular case of Model III. On the one hand, an increase in M causes an increase in δ (Eq. 11) and correspondingly, a decrease in the steady state value of y (Eq. 12). As a consequence, the intracellular pH increases (Fig. 4). A decrease in y^* would, in turn, cause, by itself, a decrease in the membrane potential (Eq. 2). However, because, on the other hand, η_0 increases with M (Eq. 3), the two effects can be balanced. For the particular set of numerical values employed in this study, for the interval explored the membrane potential increases with M (Fig. 4), in agreement with experimental evidence and with

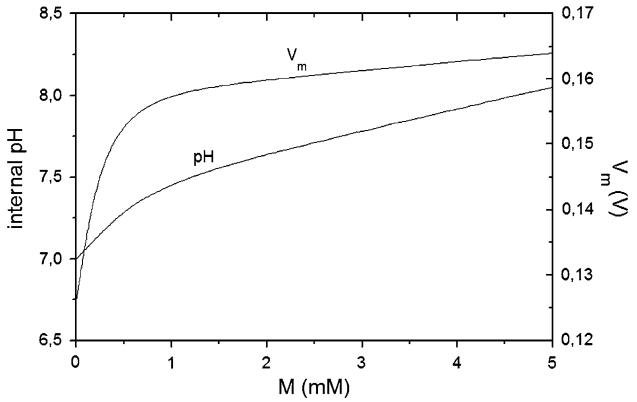

Fig. 4 Dependence of the steady state values of the internal pH and membrane potential V_m on the concentration of the additional metabolite M, for Model III. The *plots* were obtained by employing Eqs. 2, 11, and 12 and, except for M, the numerical values of the parameters shown in Table 1

the properties of more explicit models of energy coupling in the membranes of microorganisms or mitochondria (Cristina and Hernández 2000).

Effect of M on the dynamic properties of Models I and III

For the dynamic simulations, Eq. 4 (Model I) or Eq. 10 (Model III) were integrated numerically, using the Runge–Kutta fourth order method and, unless otherwise stated, the numerical values of the parameters listed in Table 1. The initial values of the variables for the simulations of Model I were given by:

$$y^* = \alpha_0 x_o/\delta_0 \text{ and } V_m^* = (RT/F)\ \ln\left(n_0\, y^*/\mu_0\, x_o\right). \qquad (18)$$

Employing Eq. 18 and the numerical values listed in Table 1, the reference condition for Model I is given by $y^* = 10^{-11}$ mol cm^{-3} (corresponding to an internal pH = 8.0) and $V_m^* = 0.166$ V. For this model, the simulated oscillations were triggered by incorporation of M at the corresponding concentration.

For Model III, the initial values for the simulations were $x(t = 0) = x^*$, $y(t = 0) = y^*(1 - \Delta y)$, and $V_m(t = 0) = V_m^*$, where the asterisk (*) denotes the corresponding steady state and where the perturbation Δy that triggered the oscillations was considered to be proportional to M ($\Delta y = 10^5 M$). The proportionality factor employed (10^5) was arbitrarily chosen to yield good numerical approximations to the experimental results. Under reference conditions (Table 1), the numerical values considered for Model III yield the results:

1 $k = r = 110$, indicating the existence of sustained oscillations with a frequency equal to 1 min^{-1} (cf. Fig. 3 and Eq. 29);
2 $y^* = 9.17 \times 10^{-12}$mol cm^{-3} (corresponding to an internal pH = 8.05); and
3 $V_m^* = 0.164$ V.

It should be noted that the reference values for the internal pH and V_m are similar for the two models.

For both models, the frequency of the oscillations was directly determined from the numerical simulations. For the particular case of Model III, these frequencies were in fair agreement with those predicted from the theoretical analysis (Eq. 29).

Figure 5 shows the oscillatory behavior of Models I and III under the reference conditions (Table 1). As can be seen, for the numerical values of the parameters chosen,

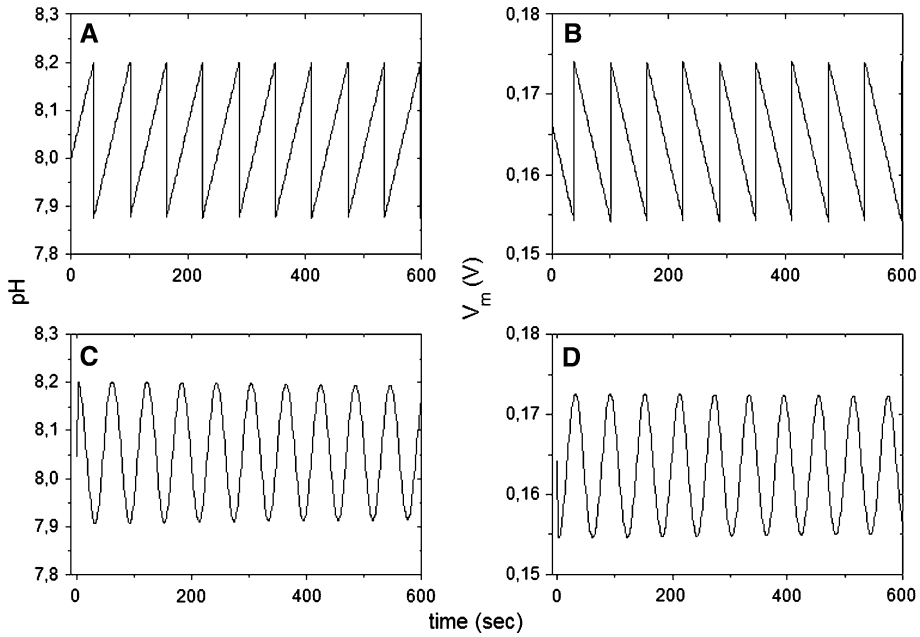

Fig. 5 Dynamic behavior of Model I (**a** and **b**) and Model III (**c** and **d**) in the presence of M at a concentration of 5 mM. The *plots* show sustained oscillations in internal pH (**a** and **c**) and V_m (**b** and **d**), obtained by numerical integration of Eqs. 4 (**a** and **b**) and 10 (**c** and **d**) and employing the numerical values of the parameters shown in Table 1 (see the main text for further details)

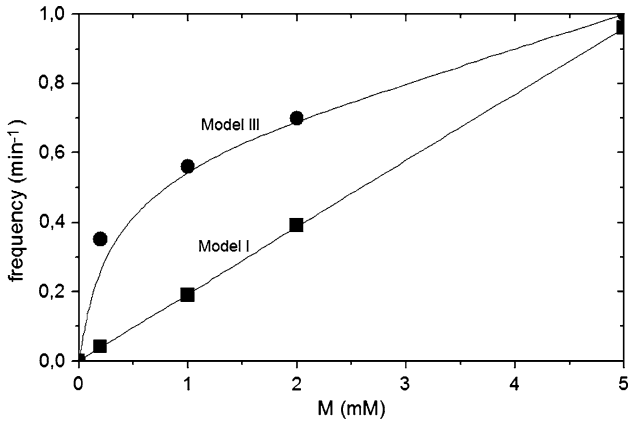

Fig. 6 Dependence of the oscillatory frequency on M, for Models I and III. The *symbols* correspond to results directly determined from the numerical simulations employing, except for M, the values of the parameters in Table 1. The curve for Model III was obtained from solution of Eq. 29

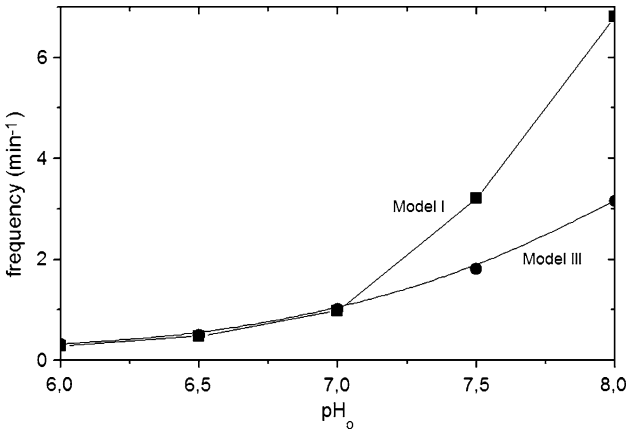

Fig. 7 Dependence of the oscillatory frequency on external pH (pH_o, obtained from x_o), for Models I and III. The *symbols* correspond to results directly determined from the numerical simulations employing, except for x_o, the values of the parameters in Table 1. The curve for Model III was obtained from solution of Eq. 29

both models are capable of exhibiting analogous oscillations in internal pH and membrane potential, consistent with the experimental evidence (HWU). In particular, for both models the oscillatory frequencies were similar and also consistent with the experimental findings of these authors.

In subsequent studies of the dependence of the oscillatory frequencies on the concentration of the metabolite (M) and the external pH (pH_o), the results of the numerical simulations of Models I and III were also compared with those obtained from the experiments by HWU. The dependence of the frequencies on M is shown in Fig. 6. In the two models the oscillation frequency increases with M, in agreement with the experimental evidence (HWU). Comparison of the results of the simulations (Fig. 6) with those obtained by these authors leads to the conclusion that Model III yields a significantly better approximation. For Model I a linear dependence can be observed; this does not reproduce the experimental evidence in the range of M values explored. The fact that the more complex Model III assumes that M affects more variables than in Model I (cf. Eqs. 5 and 11) suggests that further effects of M should be considered apart from the increase in the pumping rate δ.

Figure 7 shows the dependence of the oscillatory frequencies on external pH (pH_o). Although, in general agreement with the experimental evidence, in the two models the frequency increases with external pH, neither provides a very good approximation of the experimental results obtained by HWU. Nevertheless, the approximation obtained with Model III is somewhat better, once again suggesting that further effects on the model variables should be taken into consideration.

Taken together, the results of the numerical simulations of the models show, in general terms, that Models I and III both have properties consistent with the experimental evidence obtained by HWU about the appearance of electrical oscillations in isolated mitochondria. In this respect, it is interesting to note that the models only consider events related to the passive and active transport of protons as means of explaining the experimental data, in agreement with the interpretations made by those authors. The fact that the somewhat more involved Model III is capable of yielding better approximations to the experimental findings suggests that interpretation of the oscillatory behavior may require consideration of further effects than the elementary ones assumed in Model I. Although, as already mentioned, the effects of concurring mitochondrial processes (i.e., production of reactive oxygen species, mitochondrial calcium storage, etc.) were not taken into consideration, further refinements of the models should also include their possible roles in the triggering and modulation of the oscillations.

Other dynamic effects

We explored further numerical properties of the models which may enable the proposal of experimental maneuvers to test their accuracy. In this respect, we performed simulations to mimic the effects of inhibitors of ion conductance and active transport, for the reference value of M (5 mM, Table 1). For Model I we can see in Fig. 8a that simultaneously decreasing the two proton conductances, α_0 and α_1^0 (Eqs. 5) results in increases in both internal pH and the oscillatory frequency. The increase in pH is associated with a decrease in the intracellular concentration of protons (i.e., in y, cf. Eq. 18) whereas the increase in the oscillatory frequency is similar to that determined by an increase in external pH (cf. Fig. 7). For Model III, overall inhibition of the proton conductance was simulated by simultaneously decreasing κ, b_0, and b_1 (Eq. 11). The results (not shown)

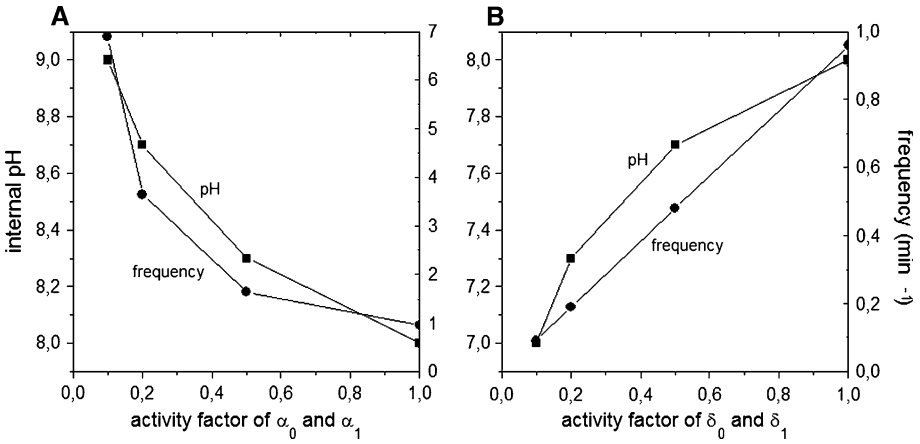

Fig. 8 Effect of decreases in α (**a**) and δ (**b**) on internal pH and oscillatory frequency for Model I. The *symbols* correspond to results directly obtained from Eq. 18 (for internal pH) or from numerical simulations (for frequency). Except for the modified parameters, the numerical values employed were those in Table 1. For each case, the parameters were modified according to the formula: activity factor × parameter. For α (δ), both α_0 (δ_0) and α_1 (δ_1) were simultaneously modified to the same extent (Eq. 5)

reveal that the decrease in those parameters determines, similarly to the case of Model I, an increase in the internal pH that can be interpreted with the aid of Eqs. 11 and 12. In addition however, that decrease determines the gradual evolution of Model III towards instability, a result that can be interpreted by demonstrating that the ratio k/r (Eq. 13) becomes progressively smaller (cf. Fig 3).

Figure 8b shows that, for Model I, the simultaneous decrease in the two components of the active proton transport rate, δ_0 and δ_1^0 (Eq. 5), determines a decrease in both the internal pH and the oscillatory frequency. The smaller pumping rate is the cause for the decrease in the internal pH, as can be interpreted from inspection of Eq. 18. The decrease in the oscillatory frequency is similar to that obtained by reducing the concentration of M (Fig. 6). For Model III, analogous inhibition of d_0 and d_1^0 (Eq. 11) causes (results not shown), similarly to the case of Model I, a decrease in the internal pH that can be interpreted with the aid of Eqs. 11 and 12. In addition, the decrease in the pumping rate determines the gradual evolution of Model III towards non-oscillatory stability, a result that can be interpreted by demonstrating that the ratio k/r (Eq. 13) becomes progressively larger (cf. Fig 3).

Taken together, the results in this section provide elements for further testing the validity of each model and distinguishing between them. To the best of our knowledge, there is still no available experimental evidence with which to test these theoretical results.

Conclusions

In this study we have introduced two relatively simple dynamic models (Model I and Model III) of electric potential oscillations in non-excitable membranes. The models primarily describe modification of the internal concentration of an ionic species mainly responsible for generation of the membrane potential. Depending upon the values chosen, the two models can yield oscillations in the ion concentration and, consequently, in the membrane potential. The models were constructed following interpretations of experimental findings in mitochondria and are plausible kinetically and mechanistically. Model I assumes that one component of the proton conductance is triggered in response to matrix alkalinization whereas Model III is a continuous model in which the oscillatory behavior depends on the existence of positive feedback regulation of the proton conductance by the matrix protons. Under reference conditions (i.e., conditions reproducing standard experimental findings) the two models yield similar oscillatory behavior. Modifications of these conditions and simulation of other effects enables prediction of different dynamic behavior of the two models, a fact potentially useful for establishing their accuracy in the interpretation of experimental data. Although in this study the models were mainly intended to reproduce findings about electric potential oscillations in mitochondria, they could also be used to represent electrical oscillations associated with calcium oscillations in mitochondria or other cellular systems, because several calcium channels have also been reported to undergo calcium modulation.

Acknowledgments Supported by grants from the Programa para el Desarrollo de las Ciencias Básicas (PEDECIBA) and from the Comisión Sectorial de Investigación Científica (CSIC), Universidad de la República, Uruguay.

Appendix 1: A simple kinetic model of a cation pump

Figure 2a depicts a simple kinetic diagram of the active transport mediated by system 1 (Fig. 1a), in which the

transport of y is coupled to the reaction $S \leftrightarrow P$. From analysis of this kinetic diagram, the net flux of transport J_p in the $y \rightarrow x_o$ direction is given by:

$$J_p = (N_p/\Sigma_p)\,(u_{01}v_{10}Sy - u_{10}v_{01}Px_o), \tag{19}$$

with $\Sigma_p = u_{10} + v_{10} + u_{01}Sy + v_{01}Px_o$.

In these expressions, N_p is the total membrane density of the enzyme; u_{01}, v_{10}, u_{10}, and v_{01} are rate constants (cf. Fig. 2a), and S, P, x_o, and y are the concentrations of the corresponding species. If the process operates in an irreversible fashion, J_p will be given by:

$$J_p = (N_p/\Sigma_p)\,(u_{01}v_{10}Sy). \tag{20}$$

Equation 20 can be identified with the term $[\delta y/(1 + \gamma y)]$ of Models II and III (Eqs. 6 and 10, respectively), with δ and γ given by:

$$\begin{aligned} &\delta = (N_p u_{01} v_{10} S)/(u_{10} + v_{10} + v_{01}Px_o) \quad \text{and} \\ &\gamma = (u_{01}S)/(u_{10} + v_{10} + v_{01}Px_o). \end{aligned} \tag{21}$$

Note that under some of the conditions in this study substrate S can be metabolite M.

Appendix 2: Derivation of expressions for the feedback effect of y from analysis of explicit kinetic models of channel activation and inactivation

Explicit kinetic schemes for the portion of ion transport mediated by system 3 (Fig. 1a) are shown in Fig. 2b, c. These kinetic models represent simple cases of channel activation (Fig. 2b) and inactivation (Fig. 2c) by the transported ligand, where the channel pre-exists in two conformational states, N_0 and N_0*, only one of which (N_0) is capable of performing net ionic transport. For channel activation (Fig. 2b), the transition from the inactive to the active state is promoted by the state "y" of the transported species. From analysis of the kinetic diagram shown in Fig. 2b, the net flux J of transport of the cation in the $x \rightarrow y$ direction is given by:

$$J = (Np/\Sigma)\,(k_{01}l_{10}xy - k_{10}l_{01}y^2). \tag{22}$$

In Eq. 22, N is the total density of the channel; p, q, k_{01}, l_{10}, k_{10}, and l_{01} are rate constants (cf. Fig. 2b); x and y are the concentrations of the corresponding species, and Σ is the sum of all the directional diagrams of the model, given by:

$$\Sigma = (p + q)\,(l_{10} + k_{10}) + py(l_{01}y + k_{01}x).$$

If the system operates irreversibly under conditions far from saturation, Eq. 22 can be approximated by:

$$J \cong [(Npk_{01}l_{10}/q)/(l_{10} + k_{10})]xy. \tag{23}$$

Equation 23 is formally analogous to the term βxy included in Model III (Eq. 10), with β given by $(Npk_{01}\,l_{10}/q)/(l_{10} + k_{10})$.

For channel inactivation by the transported species (Fig. 2c), y promotes the transition from the active (N_0) to the inactive state (N_0*). The net flux of transport J in the $x \rightarrow y$ direction is now given by:

$$J = (Ns/\Sigma)\,(k_{01}l_{10}x - k_{10}l_{01}y). \tag{24}$$

where the symbols have analogous meanings to the previous case (cf. Eq. 22). The term Σ is now given by:

$$\Sigma = s(l_{10} + k_{10} + k_{01}x) + y[sl_{01} + r(k_{10} + l_{10})].$$

If the system operates under irreversible conditions and if the term $s\,k_{01}\,x$ can be neglected, Eq. 24 can be approximated by:

$$J = (Ns/\Sigma)\,(k_{01}l_{10}x) \tag{25}$$

with $\Sigma = s(l_{10} + k_{10}) + y[sl_{01} + r(k_{10} + l_{10})]$.

Equation 25 is formally analogous with the term $\beta x/(1 + \varphi y)$ included in Model II (Eq. 6), with β and φ given by:

$$\begin{aligned} &\beta = (Nsk_{01}l_{10})/s(l_{10} + k_{10}) \quad \text{and} \\ &\varphi = [sl_{01} + r(k_{10} + l_{10})]/s(l_{10} + k_{10}). \end{aligned} \tag{26}$$

Appendix 3: Stability analysis of model II

The eigenvalues $\lambda_{1,\,2}$ of the characteristic equation of the linear approximation to the model given by Eq. 8 are

$$\lambda_{1,2} = -\theta/2 \pm \Delta^{1/2}/2,$$

with:

$$\begin{aligned} &\theta = (k + r)\,(r - 1)/r \quad \text{and} \\ &\Delta = [(k - r)(r - 1)/r]^2 + 4(k/r)(r - 1). \end{aligned} \tag{27}$$

Because Δ is necessarily positive, Model II is not capable of exhibiting oscillatory behavior.

Appendix 4: Stability analysis of model III

The eigenvalues $\lambda_{1,2}$ of the characteristic equation of the linear approximation to the model given by Eq. 14 are

$$\lambda_{1,2} = -\theta/2 \pm \Delta^{1/2}/2,$$

with:

$$\begin{aligned} &\theta = -k/(r - 1) + (r - 1)/r \quad \text{and} \\ &\Delta = \theta^2 + 4(k/r)(1 - r). \end{aligned} \tag{28}$$

If $r \gg 1$, $\theta = 1 - (k/r)$ and $\Delta = [1 - (k/r)]^2 - 4k$. If $k = r$, $\theta = 0$, and $\Delta = -4k$. Therefore, under this

condition, because k is necessarily positive, sustained oscillations occur with the period T given by:

$$T = 2\pi/k^{1/2} \quad (29)$$

References

Aidley DJ, Stanfield PR (1996) Ion channels. Molecules in action. Cambridge University Press, Cambridge, p 152

Bauer CS, Simonis W, Schonknecht G (1999) Different xanthines cause membrane potential oscillations in a unicellular green alga pointing to a ryanodine/cADPR receptor Ca^{2+} channel. Plant Cell Physiol 40:453–456

Beard DA (2005) A biophysical model of the mitochondrial respiratory system and oxidative phosphorylation. PLoS Comput Biol 1(4):e36

Bergsten P (2002) Role of oscillations in membrane potential, cytoplasmic Ca^{2+}, and metabolism for plasma insulin oscillations. Diabetes 51:S171–S176

Bertram R, Pedersen MG, Luciani DS, Sherman A (2006) A simplified model for mitochondrial ATP production. J Theor Biol 243:575–586

Brand MD, Felber SM (1984) Membrane potential of mitochondria in intact lymphocytes during early mitogenic stimulation. Biochem J 217:453–459

Chalmers S, McCarron JG (2008) The mitochondrial membrane potential and Ca^{2+} oscillations in smooth muscle. J Cell Sci 121:75–85

Chen LB (1988) Mitochondrial membrane potential in living cells. Ann Rev Cell Biol 4:155–181

Cortassa S, Aon MA, Winslow RL, O'Rourke B (2003) An integrated model of cardiac mitochondrial energy metabolism and calcium dynamics. Biophys J 84:2734–2755

Cortassa S, Aon MA, Marban E, Winslow RL, O'Rourke B (2004) A mitochondrial oscillator dependent on reactive oxygen species. Biophys J 87:2060–2073

Cristina E, Hernández JA (2000) An elementary kinetic model of energy coupling in biological membranes. Biochim Biophys Acta 1460:276–290

Decoursey TE (2003) Voltage-gated proton channels and other proton transfer pathways. Physiol Rev 83:475–579

Hanley PJ, Musset B, Renigunta V, Limberg SH, Dalpke AH, Sus R, Heeg KM, Preisig-Müller R, Daut J (2004) Extracellular ATP induces oscillations of intracellular Ca^{2+} and membrane potential and promotes transcription of IL-6 in macrophages. Proc Natl Acad Sci USA 101:9479–9484

Hattori T, Watanabe K, Uechi Y, Yoshioka H, Ohta Y (2005) Repetitive transient depolarizations of the inner mitochondrial membrane induced by proton pumping. Biophys J 88:2340–2349

Hernández JA (2003) Stability properties of elementary dynamic models of membrane transport. Bull Math Biol 65:175–197

Hernández JA, Fischbarg J, Liebovitch LS (1989) Kinetic model of the effects of electrogenic enzymes on the membrane potential. J Theor Biol 137:113–125

Higgins J (1964) A chemical mechanism for oscillation of glycolytic intermediates in yeast cells. Proc Natl Acad Sci USA 51: 989–994

Higgins J (1967) The theory of oscillating reactions. Ind Eng Chem 59:18–62

Krippeit-Drews P, Düfer M, Drews G (2000) Parallel oscillations of intracellular calcium activity and mitochondrial membrane potential in mouse pancreatic B-cells. Biochem Biophys Res Comm 267:179–183

Lang F, Friedrich F, Kahn E, Woll E, Hammerer M, Waldegger S, Maly K, Grunicke H (1991) Bradykinin-induced oscillations of cell membrane potential in cells expressing the Ha-ras oncogene. J Biol Chem 266:4938–4942

Lee A, Catterall WA (2005) Ca^{2+}-dependent modulation of voltage-gated Ca^{2+} channels. In: Zamponi GW (ed) Voltage-gated calcium channels. Kluwer, New York, pp 183–193

Magnus G, Keizer J (1998) Model of beta-cell mitochondrial calcium handling and electrical activity. I. Cytoplasmic variables. Am J Physiol 274:C1158–C1173

Manning Fox JE, Gyulkhandanyan AV, Satin LS, Wheeler MB (2006) Oscillatory membrane potential response to glucose in islet β-cells: a comparison of islet-cell electrical activity in mouse and rat. Endocrinology 147:4655–4663

McDonald AG (2003) Implications of enzyme kinetics. Biochem Soc Trans 31:719–722

Miller JB, Koshland DE Jr (1977) Sensory electrophysiology of bacteria: relationship of the membrane potential to motility and chemotaxis in *Bacillus subtilis*. Proc Natl Acad Sci USA 74:4752–4756

Nicholls DG, Budd SL (2000) Mitochondria and neuronal survival. Physiol Rev 80:315–360

Nicholls DG, Ferguson SJ (2002) Bioenergetics 3. Academic Press, London

Nunemaker CS, Bertram R, Sherman A, Tsaneva-Atanasova K, Daniel CR, Satin LS (2006) Glucose modulates $[Ca^{2+}]_i$ oscillations in pancreatic islets via ionic and glycolytic mechanisms. Biophys J 91:2082–2096

Tedeschi H (1974) Mitochondrial membrane potential: evidence from studies with a fluorescent probe. Proc Nat Acad Sci USA 71:583–585

Thomas GR, Duncan G, Sanderson J (1998) Acetylcholine-induced membrane potential oscillations in the intact lens. Invest Ophthalmol Vis Sci 39:111–119

Tilly BC, Tertoolen LJG, Lambrechts AC, Remorie R, de Laat SW, Moolenaar WH (1990) Histamine-Hl-receptor-mediated phosphoinositide hydrolysis, Ca^{2+} signalling and membrane-potential oscillations in human HeLa carcinoma cells. Biochem J 266:235–243

Vergun O, Reynolds IJ (2004) Fluctuations in mitochondrial membrane potential in single isolated brain mitochondria: modulation by adenine *n*Nucleotides and Ca^{2+}. Biophys J 87:3585–3593

Vergun O, Votyakova TV, Reynolds IJ (2003) Spontaneous changes in mitochondrial membrane potential in single isolated brain mitochondria. Biophys J 85:3358–3366